Vietnam Journal of Earth Sciences, 48(3), 353−370, https://doi.org/10.15625/2615-9783/24315

Vietnam Journal of Earth Sciences
https://vjs.ac.vn/index.php/jse

Comparison of PlanetScope and Sentinel-2 satellite observations in mapping small-scale forest fires

Pham Duc Binh[1*], Nguyen Manh Hung[2,3], Teodosio Lacava[4]

[1]*REMOSAT, University of Science and Technology of Hanoi, VAST, Hanoi, Vietnam*
[2]*Vietnam National Space Center, VAST, Hanoi, Vietnam*
[3]*Graduate University of Science and Technology, VAST, Hanoi, Vietnam*
[4]*Institute of Methodologies for Environmental Monitoring (IMAA), National Research Council (CNR), Tito Scalo, Italy*

Received 11 November 2025; Received in revised form 07 January 2026; Accepted 09 March 2026

ABSTRACT

This study evaluates the performance of multispectral optical sensors onboard PlanetScope (PS) and Sentinel-2 satellites in mapping burned areas resulting from a small forest fire that occurred on 21 March, 2025, in Nghiem Mountain, northern Vietnam. Cloud-free pre- and post-fire imagery acquired on the same dates (17 January and 12 May, 2025) were used to compute the difference Normalized Difference Vegetation Index (dNDVI) using Red and Near-Infrared surface reflectance. A threshold value (T = 0.10), selected after analyzing the dNDVI histograms, was applied to classify burned (dNDVI > T) and unburned regions (dNDVI ≤ T). Results showed a strong spatial correlation between dNDVI maps derived from both satellites (R = 0.97), although Sentinel-2 tends to yield slightly higher dNDVI values than PS satellites. The burned area estimated from PS was 20.622 ha, while Sentinel-2 produced a similar estimate of 20.225 ha, a difference of less than 2% and in close agreement with the official damage assessment report (~20 ha). Most discrepancies occurred along fire boundaries, where mixed pixels and spectral heterogeneity are expected. Our results demonstrate the effectiveness of Sentinel-2 and PS satellite imagery for mapping burned areas from small-scale fires, which is essential for forest management. Despite several limitations, including dependence on clear-sky conditions and the lack of a ground-based validation dataset, the proposed approach provides a timely and cost-effective solution for wildfire mapping at small scales, particularly important in remote regions.

Keywords: Wildfire mapping, NDVI, dNDVI, PlanetScope, Sentinel-2, Vietnam.

1. Introduction

Wildfires are uncontrolled, destructive fires that spread rapidly through forests, grasslands, woodlands, or brush. They occur thousands of times each year across all continents and represent one of the most widespread natural hazards worldwide (Gibson et al., 2020; P. Pereira et al., 2021). Their impacts have become increasingly severe as climate change has intensified environmental stress, particularly through rising temperatures and prolonged droughts (Marín et al., 2018; Paquette et al., 2018). Recent satellite-based studies have estimated that approximately 4 million km^2 of land are burned each year globally (Chuvieco et al., 2018). Although there has been a 27% global decline in burned areas over the last two

*Corresponding author, Email: pham-duc.binh@usth.edu.vn

decades (Jones et al., 2022), the frequency and intensity of large fires are expected to increase in the future, notably in regions such as North and South America, Australia, and Southern Europe (Moreira et al., 2020; Radeloff et al., 2018; Seydi et al., 2021). Wildfires play a critical role in climate change and the global carbon cycle by emitting large quantities of greenhouse gases to the atmosphere, potentially reinforcing climate warming through positive feedback loops (Zhang et al., 2024).

Additionally, wildfires can lead to the destruction of forests, short- and long-term disruption of biodiversity, soil degradation, air pollution, disruption of water cycles, and threats to human lives and infrastructure. Accurate burned-area mapping is essential for monitoring the spatial extent and severity of wildfires, which is important for post-fire recovery efforts (Pham-Duc & Nguyen, 2024; Pham Thanh et al., 2024). Such information also supports land management, fire prevention planning, and climate modeling by providing critical data on fire frequency and spatial distribution over time (Or et al., 2023).

Traditional burned-area assessments rely heavily on field surveys and administrative reports (Mouillot & Field, 2005; Nguyen Thanh et al., 2025). While ground observations remain valuable, they are often labor-intensive, time-consuming, and impractical for large or remote fire-affected regions (Chuvieco et al., 2019). Moreover, inconsistencies in data collection and methods across countries and agencies make it difficult to integrate such data for regional or global analyses (Chuvieco et al., 2018). To address these limitations, satellite imagery has been used for burned-area mapping since the 1970s, as satellites provide timely, consistent, and cost-effective alternatives to field surveys. One of the first publications, presented shortly after the launch of Landsat-1 in 1972 at a conference, highlighted the potential of satellite imagery for burned-area mapping (Hitchcock & Hoffer, 1974). Since then, satellite observations have become widely adopted for fire monitoring, using spectral indices such as the Normalized Burn Ratio (NBR) or the Normalized Difference Vegetation Index (NDVI) (Key & Benson, 2003; Suárez-Fernández et al., 2025).

Different satellite systems support burned area mapping at various spatial and temporal scales. At global and continental levels, coarse-resolution sensors such as the Moderate Resolution Imaging Spectroradiometer (MODIS) and the Visible Infrared Imaging Radiometer Suite (VIIRS) are widely used due to their frequent revisit times (Chen et al., 2023; Giglio et al., 2018; Ouattara et al., 2024; A. A. Pereira et al., 2017). However, their coarse spatial resolution often leads to high omission errors in their estimates, particularly for small and fragmented burned areas (Liu et al., 2023). For regional-scale applications, medium-resolution sensors such as Landsat and the Sentinel-2 series (10–30 m) provide more detailed burned-area assessments (Hawbaker et al., 2020; Howe et al., 2022; Suwanprasit & Shahnawaz, 2024). However, mapping burned areas with these sensors is limited by their infrequent revisit times, making it challenging in areas with high cloud cover, such as tropical regions (Liu et al., 2023). The introduction of cloud computing platforms, such as Google Earth Engine (GEE), has revolutionized satellite data processing, making it more accessible and efficient (Gorelick et al., 2017). Recently, the GEE platform has been widely used for many monitoring applications in Earth sciences

(Pham-Duc et al., 2023), including burned-area monitoring and mapping (Konkathi & Shetty, 2021). Recently, some scholars used GEE to combine data from multiple satellite sensors to enhance the accuracy of burned area detection (Bar et al., 2020; Bastarrika et al., 2024). For small-scale fires (<30 ha), very high-resolution commercial satellite imagery (e.g., PlanetScope (PS), Geoeye-1, Worldview-2, and QuickBird-2) is ideal as they can provide sub-meter spatial resolution maps (Dragozi et al., 2015; Palandjian et al., 2009; Pham-Duc, 2023; Vanderhoof et al., 2018). However, access to such data is often restricted due to financial constraints. To overcome cloud-related limitations in optical systems, recent research has explored data fusion techniques that integrate optical and radar satellite images for more robust burned-area mapping (Lasko, 2021; Nguyen Cong et al., 2024; Zhang et al., 2021, 2024).

The objective of this study is to evaluate and compare the effectiveness of Sentinel-2 and PS optical imagery for mapping burned areas resulting from a small forest fire which occurred on 21 March, 2025, in Nghiem Mountain, northern Vietnam. The results contribute to both regional and global literature on burned area mapping using moderate- and high-resolution satellite imagery. In addition, the findings provide valuable information for local authorities involved in post-fire damage assessment and land management planning. Following the introduction, Section 2 provides a detailed description of the study area and the main characteristics of the Sentinel-2 and PS data used. Section 3 presents the methodology employed to process and analyze satellite imagery. The main results are presented in Section 4, followed by a discussion in Section 5. Finally, Section 6 concludes the study by summarizing our main findings, highlighting key limitations, and proposing potential ideas for future work in this research direction.

2. Study area and Materials

2.1. Study area

Nghiem Mountain, located in Hoang Khai commune, Tuyen Quang province, northern Vietnam (Fig. 1a), reaches a maximum elevation of approximately 470–480 m above sea level. A forest fire broke out in the area at around 11:00 on 21 March, 2025. The affected forest, primarily bamboo, was highly flammable, and the combination of dry weather and strong winds caused the fire to spread rapidly and widely, posing significant challenges for firefighting forces. By 16:00 on the same day, the fire had largely been contained but continued to flare up within the fire barriers established by the local authorities. By 08:00 on 22 March, the fire was completely extinguished. According to the Tuyen Quang People's Committee, the forest fire resulted in one fatality and destroyed more than 20 hectares (ha) of the forest (Lao-Dong, 2025). Figures 1b and 1c show the true color composite images of the fire-affected area, derived from PS satellite observations before and after the fire event, respectively. In Fig. 1c, the burned area is clearly visible in the central portion of the scene. To enhance visual discrimination and highlight burned vegetation, Figures 1d and 1e present false-color composites obtained using PS bands, with Band 4 (NIR) assigned to the red channel, Band 3 (Red) to the green channel, and Band 2 (Blue) to the blue channel. The ENVI software (version 5.0) was used to produce these images. In the post-fire false-color composite (Fig. 1e), burned areas appear in dark green, contrasting with the bright red tones of healthy vegetation.

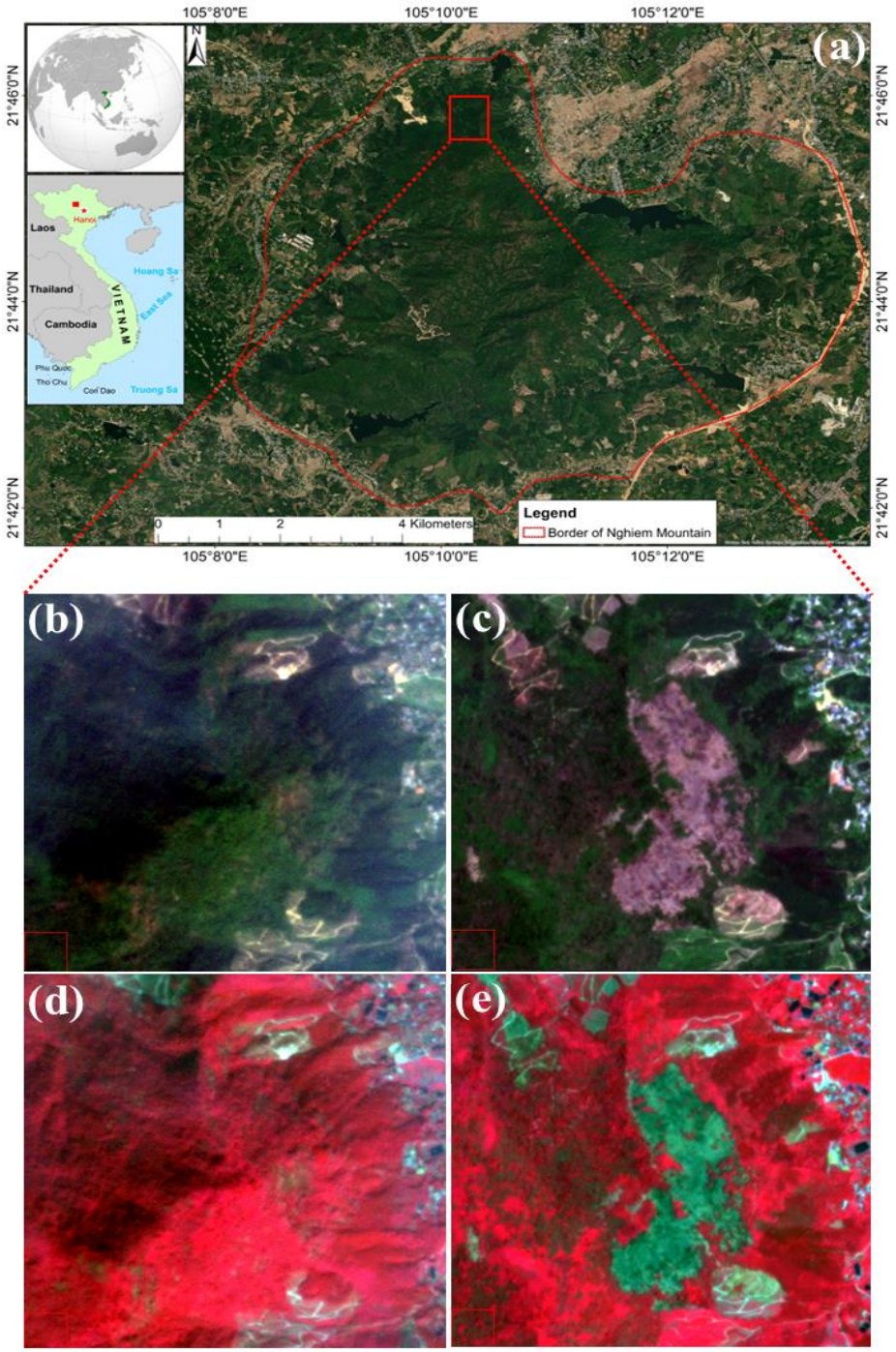

Figure 1. (a) Location of Nghiem Mountain in Tuyen Quang province, northern Vietnam (the red box in the small Vietnam map on the bottom left). The fire-affected area is inside the red square. (b & c) true color composite, and (d & e) false color composite maps of the study area before (left) and after the fire (right), derived from PS imagery

2.2. PlanetScope satellite imagery

The PS satellite constellation, operated by Planet Labs Inc., consists of a fleet of nanosatellites known as "Doves", designed to provide high-resolution, high-frequency optical imagery of Earth's surface. Since the launch of the first Doves satellites, Planet Labs Inc. has launched successfully over 450 nanosatellites across multiple generations, including the first-generation Dove Classic (launched from 2016), the second-generation Dove-R (launched from 2018), and the third and latest-generation SuperDove series (launched from April 2019). These PS satellites operate in Sun-synchronous orbit at an altitude of approximately 475 km above sea level, with an orbital inclination of 98°, completing an orbit every 90 minutes (Pham-Duc et al., 2025). The early generations of the Dove satellites were equipped with four-band multispectral sensors (Red, Green, Blue, and NIR), whereas the latest SuperDove units feature eight-band multispectral sensors. Depending on the sensors and generations, PS satellites offer a spatial resolution ranging from 3 to 12 m, with varying swath widths. Further technical details on the three PS generations and their spectral characteristics can be found in earlier review studies (Frazier & Hemingway, 2021).

In this study, two cloud-free PS Level 3B Ortho Analytic surface reflectance images with a 3-m spatial resolution were used. These images were provided free of charge by Planet Labs Inc. through the Planet's Education and Research Program (https://www.planet.com/industries/education-and-research/), which supports scientific and educational use of PS imagery. The PS dataset includes one image acquired before the fire event and another after the event. Details of the image acquisitions are provided in Table 1. The pre-fire image was captured on 17 January, 2025, at 03:45:56 UTC, approximately two months before the fire, while the post-fire image was captured on 12 May, 2025, at 03:54:09 UTC, nearly two months after the event. Both images were acquired by similar sensors onboard two different SuperDove satellites, resulting in acquisition times that differ by about 10 minutes. For this study, the Red band (650–680 nm) and NIR band (845–885 nm) were used to compute the NDVI to assess vegetation changes associated with the forest fire.

Table 1. Detailed information on pre- and post-fire PS imagery is utilized in this study

	PS Acquisition Date	**Area Coverage**	**Cloud Cover**	**Pixel Resolution**	**Instrument**	**Bands used (wavelengths)**
Pre-fire Imagery	17/01/2025 (03:45:56 UTC)	100%	0%	3 m	SuperDove (PSB.SD)	Red (650–680 nm) NIR (845–885 nm)
Post-fire Imagery	12/05/2025 (03:54:09 UTC)	100%	0%			

2.3. Sentinel-2 satellite imagery

Sentinel-2 is an optical satellite mission under the European Union's Copernicus program, consisting of three Sun-synchronous satellites: Sentinel-2A (launched in June 2015), Sentinel-2B (launched in March 2017), and Sentinel-2C (launched in September 2024). These three satellites operate at an altitude of approximately 786 km above sea level and, together, provide a global revisit time of 5 days, with a higher frequency (2-3 days) over mid-latitudes. Each Sentinel-2 satellite is equipped with the Multispectral Instrument (MSI), which acquires imagery across 13 spectral bands, ranging from the visible (400 nm) to the short-wave infrared wavelengths (SWIR; 2200 nm). Depending on the wavelengths, the MSI offers three spatial resolutions: 10, 20, and 60 m. Detailed

technical descriptions of Sentinel-2 satellites and their spectral characteristics can be found in earlier review studies (Spoto et al., 2012).

In this study, two cloud-free Sentinel-2 Level-2A Bottom-Of-Atmosphere (BOA) images with a 10-m spatial resolution were used. Similar to the PS dataset, the Sentinel-2 dataset includes one image acquired before and another acquired after the event. The acquisition details are summarized in Table 2. Both Sentinel-2 images were captured on the same dates as the PS images (17 January, 2025 and 12 May, 2025) and acquired at exactly 03:42:20 UTC by the same sensor. The GEE cloud-based platform (Gorelick et al., 2017) was used to extract and process the Red (650–680 nm) and NIR (785–900 nm) bands from Sentinel-2 satellite imagery to calculate the NDVI and assess vegetation damage caused by the forest fire.

Table 2. Detailed information on the pre- and post-fire Sentinel-2 imagery utilized in this study

	Sentinel-2 Acquisition Date	**Area Coverage**	**Cloud Cover**	**Pixel Resolution**	**Instrument**	**Bands used (wavelengths)**
Pre-fire Imagery	17/01/2025 (03:42:00 UTC)	100%	0%	10 m resampling to 3 m	MultiSpectral Instrument (MSI)	Red (650–680 nm) NIR (785–900 nm)
Post-fire Imagery	12/05/2025 (03:42:20 UTC)	100%	0%			

3. Methodology

The method applied in this study was adapted from (Pham-Duc & Nguyen, 2024), where it was originally implemented only on PS data. In this work, we extended the approach to include Sentinel-2 imagery, thereby implementing a multi-sensor framework. Integrating both Sentinel-2 and PS data required reassessing the threshold selection with a broader multi-sensor perspective. Figure 2 summarizes all the processing steps of the integrated workflow. First, a predefined shapefile of Nghiem Mountain (Fig. 1) was used to spatially subset both the pre- and post-fire images, ensuring identical spatial coverage across the two datasets. To harmonize spatial resolution, Sentinel-2 imagery (originally at 10 m) was resampled to 3 m using the *resample* function on the GEE platform, matching the native resolution of PS imagery. Second, the pre- and post-fire NDVI maps were generated using surface reflectance values from the Red and NIR bands (see Equations (1) and (2)). Specifically, PS's band 3 (Red) and band 4 (NIR), and Sentinel-2's band 4 (Red) and band 8 (NIR) were used. Third, the resulting NDVI maps were stacked using the *Layer Stacking* tool in ENVI software. All stacked NDVI images were projected in the WGS-84 coordinate system, with uniform spatial resolution (3 m) and dimensions (3203 × 2761 pixels). Fourth, the difference of the NDVI (dNDVI) was computed from the pre- and post-fire NDVI using Equations (3) and (4) for PS and Sentinel-2 imagery, respectively. Fifth, a threshold value (T = 0.10) was applied to classify pixels into two clusters: burned pixels (dNDVI > T, coded as 1) and unburned pixels (dNDVI ≤ T, coded as 0). Pixels exceeding the threshold T were considered to exhibit significant vegetation loss associated with fire damage. This threshold was determined through careful manual inspection of the dNDVI maps and their histograms, and it is consistent with thresholds utilized for mapping burned area in other studies (Kim et al., 2019; UN-SPIDER, 2023; Vetrita et al., 2025). Next, the classification maps were post-processed to correct potential misclassifications, such as pixels having significant NDVI reduction caused by seasonal vegetation dynamics rather than by fire. The final maps were then reprojected from WGS-84 to Geographic Lat/Lon

coordinate systems to enable integration into Google Earth for visualization. Finally, the two burned-area maps, derived independently from PS and Sentinel-2 imagery, were compared to perform cross-validation and assess their spatial consistency.

$$NDVI_{PS} = \frac{NIR_{PS} - RED_{PS}}{NIR_{PS} + RED_{PS}} = \frac{BAND\ 4_{PS} - BAND\ 3_{PS}}{BAND\ 4_{PS} + BAND\ 3_{PS}} \quad (1)$$

$$NDVI_{S2} = \frac{NIR_{S2} - RED_{S2}}{NIR_{S2} + RED_{S2}} = \frac{BAND\ 8_{S2} - BAND\ 4_{S2}}{BAND\ 8_{S2} + BAND\ 4_{S2}} \quad (2)$$

$$dNDVI_{PS} = NDVI_{pre-PS} - NDVI_{post-PS} \quad (3)$$

$$dNDVI_{S2} = NDVI_{pre-S2} - NDVI_{post-S2} \quad (4)$$

4. Results

4.1. Burned area mapping based on the NDVI derived from PlanetScope imagery

The pre- and post-fire NDVI maps derived from PS imagery are shown in Fig. 3. Before the fire, 71.98% of the area exhibited NDVI values greater than 0.5, while 28.02% had NDVI values below this threshold. After the fire, 88.17% of the area had NDVI values above 0.5, while only 11.83% remained below 0.5. This NDVI increase is consistent with the seasonal vegetation growth that typically occurs between January and May in northern Vietnam. However, within the burned areas, NDVI values noticeably decreased compared to the pre-fire image, resulting in very low NDVI signals (represented in yellow to red), in contrast to the high NDVI values of the surrounding unburned vegetation (shown in light to dark blue).

The dNDVI map derived from PS imagery is shown in Fig. 4 (left panel), where burned areas are clearly visible in yellow to red tones at the center of the map, standing out against the blue-colored areas of unchanged vegetation. After applying the threshold (T = 0.10) and removing misclassification pixels (pixels with significant NDVI reductions caused by seasonal vegetation dynamics rather than by the fire), the final burned area map was produced and shown in Fig. 4 (right panel). The total burned area estimated from PS imagery is approximately 20.622 ha.

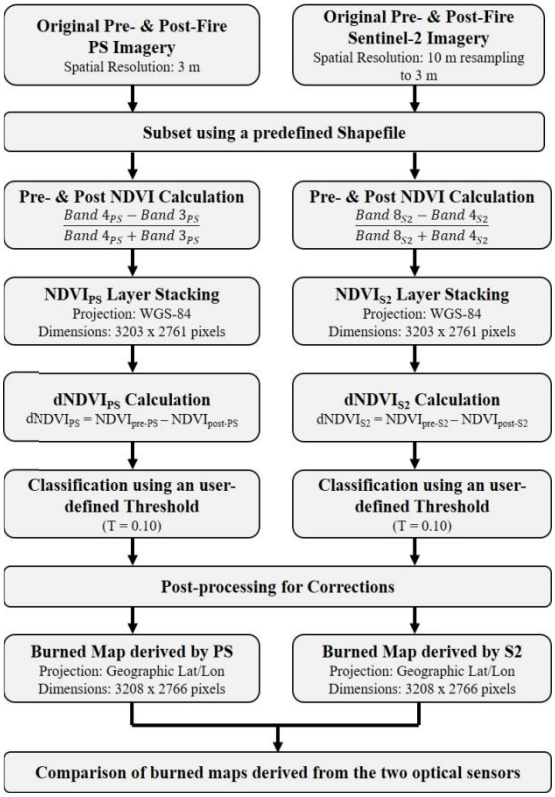

Figure 2. The flowchart used in this study to process PS and Sentinel-2 imagery, adapted from (Pham-Duc & Nguyen, 2024)

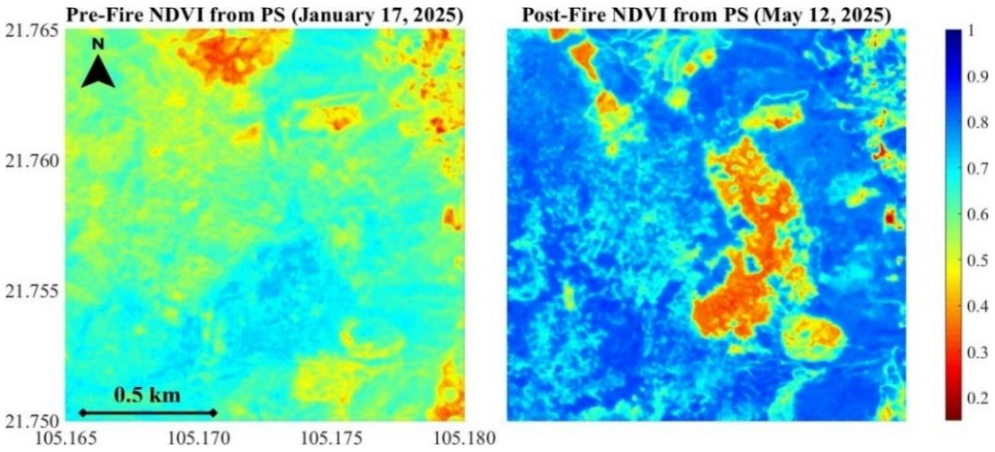

Figure 3. Pre- (left) and Post-fire NDVI maps (right) of the study area, derived from PS observations

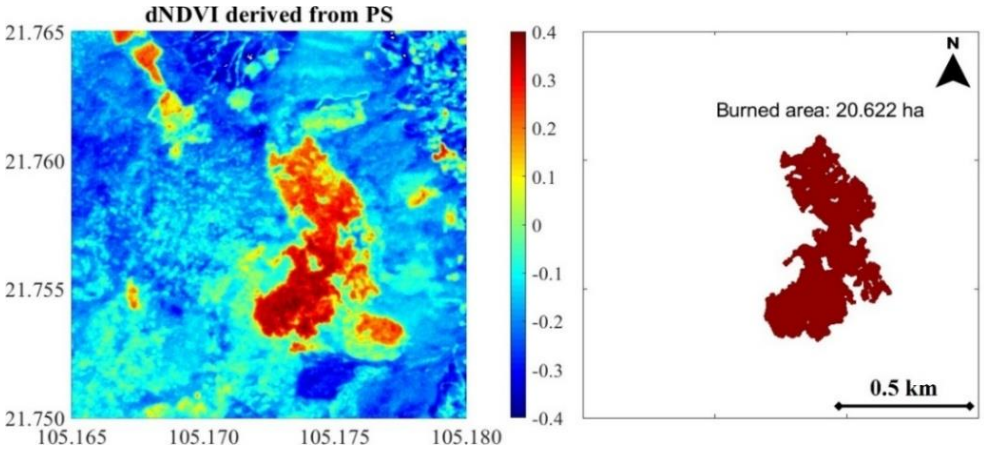

Figure 4. The dNDVI map (left) and the corresponding classified burned area map (right), derived from the PS observation

4.2. Burned area mapping based on the NDVI derived from Sentinel-2 imagery

Similar to Fig. 3, Fig. 5 presents the pre- and post-fire NDVI maps derived from Sentinel-2. Owing to differences in spectral characteristics and spatial resolution between the two sensors, the NDVI distributions are not identical. In the pre-fire map, only 14.54% of the study area had NDVI values greater than 0.5, while 85.46% had values below 0.5. In contrast, the post-fire map shows that 77.57% of the study area had NDVI values above 0.5, reflecting seasonal vegetation growth, while 22.43% remained below this threshold. However, within the burned areas, NDVI remained significantly lower (represented in red) than in the surrounding healthy vegetation (represented in blue), which had much higher NDVI values. Figure 6 is similar to Fig. 4 shows the Sentinel-2 dNDVI map (left panel). Applying the same threshold (T = 0.10) and correcting for potential seasonal misclassification resulted in the burned-area map shown in Fig. 6 (right panel). The total burned area estimated from Sentinel-2 imagery is approximately 20.225 ha.

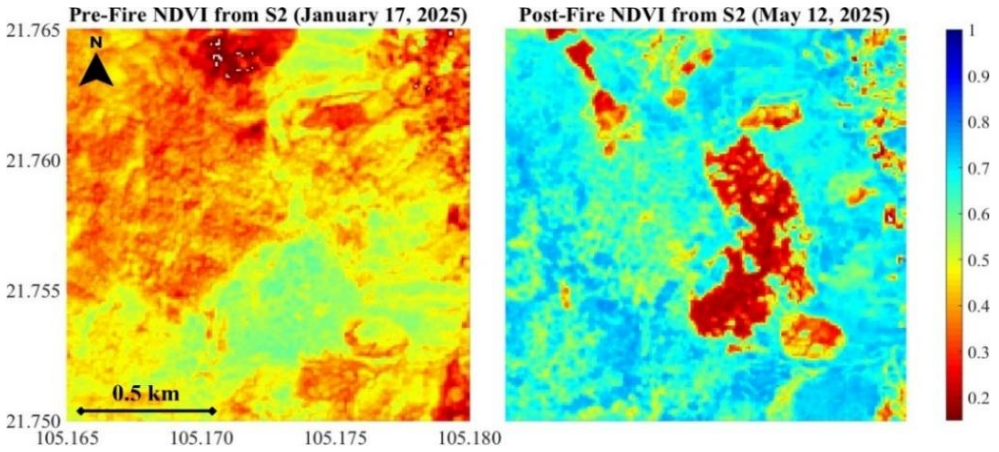

Figure 5. Pre- (left) and Post-fire NDVI maps (right) of the study area, derived from Sentinel-2 observations

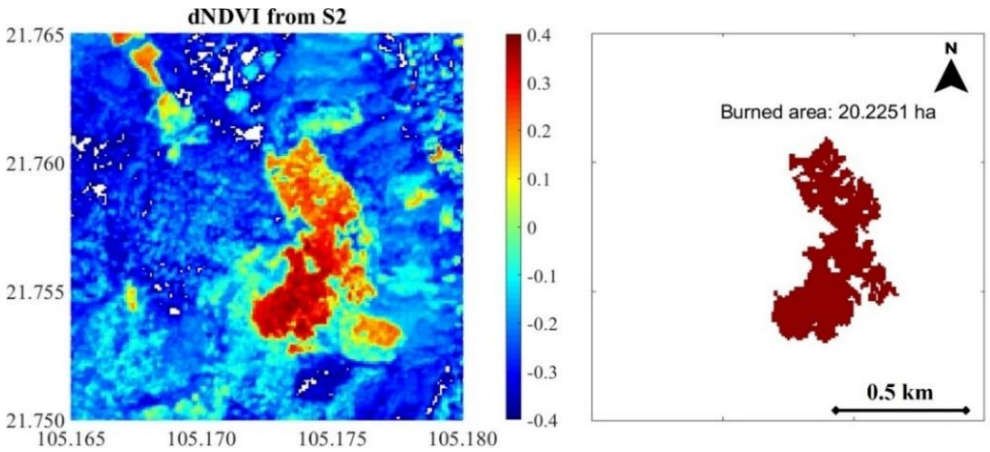

Figure 6. The dNDVI map (left) and the corresponding classified burned area map (right), derived from Sentinel-2 observation

4.3. Comparison between burned areas derived from PS and Sentinel-2 imagery

Figure 7 presents a comparison of the PS- and Sentinel-2-derived dNDVI maps. The spatial patterns of both maps are highly consistent, with high dNDVI values observed in the burned areas and low values in the surrounding unburned vegetation. Figure 8a illustrates the scatter plot of dNDVI values extracted from these two maps, revealing a very strong linear correlation (R = 0.97). The linear equation describing the relationship between the two parameters is $dNDVI_{S2} = 1.09 \times dNDVI_{PS} - 0.05$, indicating that dNDVI values derived from Sentinel-2 imagery tend to be systematically higher than those from PS imagery.

As presented in Fig. 4 and Fig. 6, the burned areas estimated from PS and Sentinel-2 imagery are 20.622 and 20.225 ha, respectively. The difference between the two estimates is less than 2%, and both are close to the official number of approximately 20 ha reported by local authorities (Lao-Dong, 2025). Figure 8b illustrates the spatial agreement between the two burned-area maps: red pixels denote burned areas detected by both sensors, green pixels are detected only by Sentinel-2, and blue pixels only by PS. The

jointly identified burned area amounts to 19.4148 ha (approximately 94% of the total), while burned areas uniquely detected by Sentinel-2 and PS are 0.8103 ha and 1.2073 ha, respectively. The discrepancies between the two maps are mostly located along transition zones between burned and unburned vegetation, where mixed pixels and spectral heterogeneity commonly introduce uncertainty. For visualization purposes, the two burned area maps were reprojected to the Geographic Lat/Lon coordinate system and exported as .kmz files for being displayed in Google Earth Pro (Fig. 9). The visualization again confirms that the two burned maps exhibit a strong spatial correlation, with the burned areas mainly located on the eastern slopes of Nghiem Mountain.

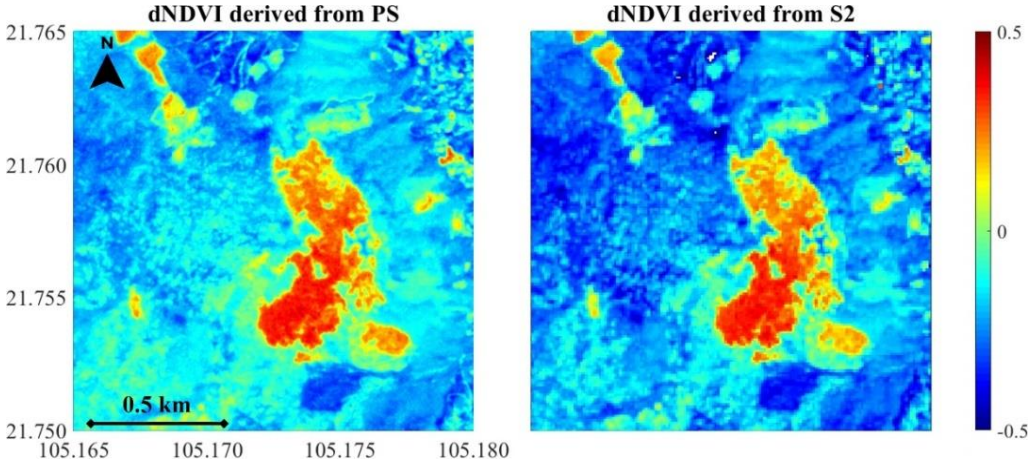

Figure 7. Comparison of the dNDVI maps derived from PS (left panel) and Sentinel-2 (right panel) observations

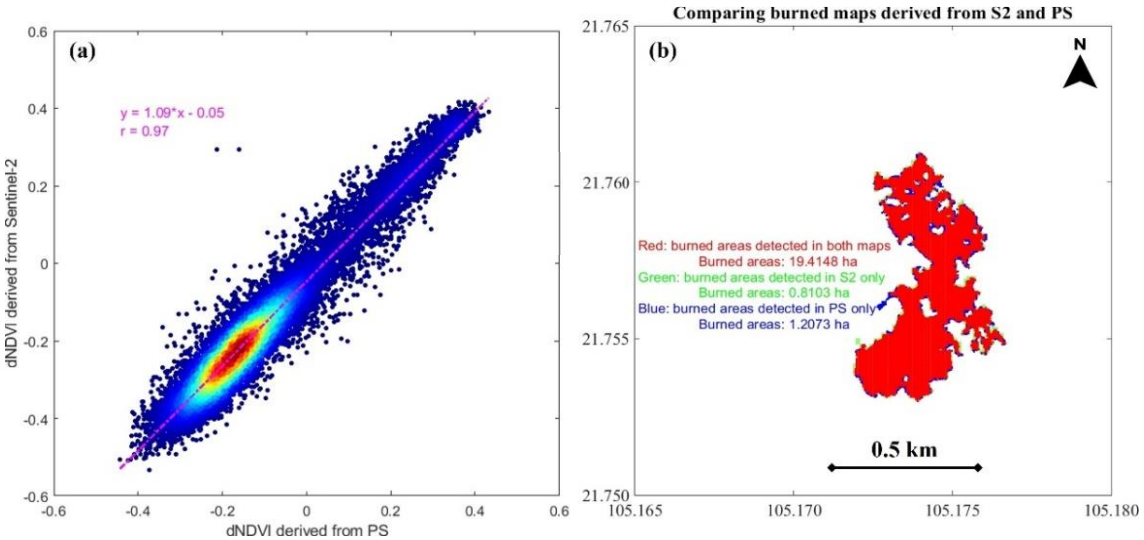

Figure 8. (a) A scatter plot shows a positive correlation between dNDVI maps derived from PS and Sentinel-2, as shown in Fig. 7. (b) Comparison between burned area maps derived from PS and Sentinel-2 observation

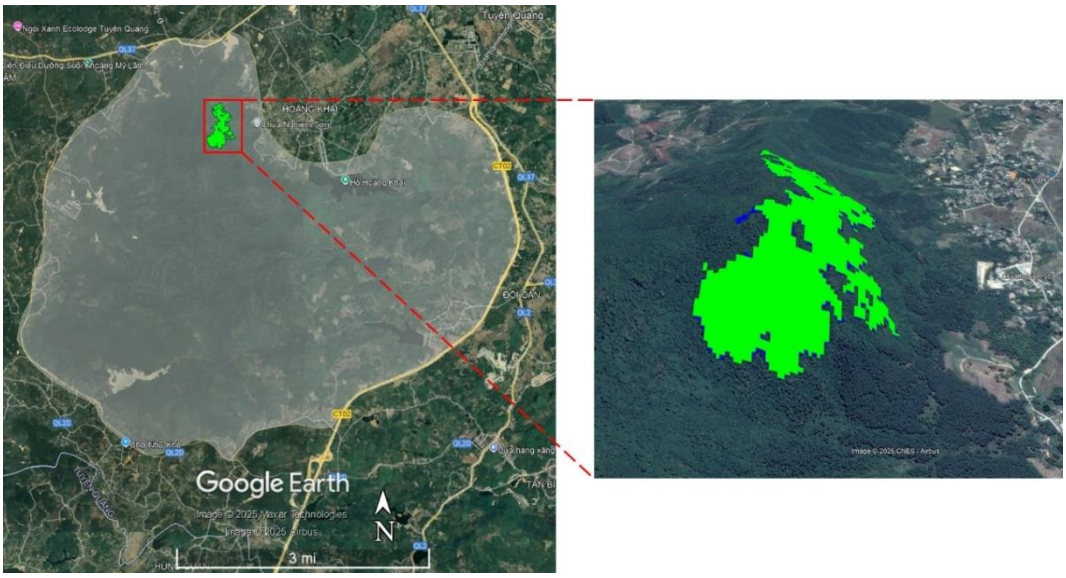

Figure 9. Burned area maps derived from PS imagery (blue) and Sentinel-2 (green), as shown in Google Earth Pro

5. Discussions

Accurate burned-area mapping at fine spatial resolution is essential for understanding wildfire behavior and impacts, even in events of very limited extent (Liu et al., 2023). Small fires typically produce highly heterogeneous burn patterns, with charred, partially burned, and unburned patches occurring in proximity. Such fine-scale variability produces subtle, spatially fragmented spectral signatures that medium- or coarse-resolution sensors may fail to capture effectively (Balakavi et al., 2025). In this context, the limitations of SWIR-based indices, such as NBR or dNBR, become evident. Although these indices are well established for larger, more homogeneous burns (Amos et al., 2019; Szpakowski & Jensen, 2019), their performance is strongly constrained by the spatial resolution of SWIR bands. In Sentinel-2, SWIR data are natively acquired at 20 m, a scale at which the small, irregular burn scars examined in this study becomes indistinguishable from surrounding vegetation, soil, and shadow components. This mixing reduces the radiometric contrast typically exploited to discriminate burned surfaces, and the enhancement attempts performed in this work did not sufficiently isolate the fire signal.

Compared with the authors' previous work, which relied exclusively on PS imagery (Pham-Duc & Nguyen, 2024), the present analysis introduces several new considerations. Integrating both Sentinel-2 and PS required reassessing threshold selection with a broader multi-sensor perspective. The two sensor systems differ in radiometric calibration, spectral bandwidth, spatial resolution, and sampling strategy. Consequently, thresholds effective for PS cannot be directly applied to Sentinel-2 without adaptation. This multi-sensor approach therefore offers a more generalizable framework, demonstrating that cross-sensor consistency depends not only on the spectral information but also on the spatial and radiometric properties of the sensors involved. In any case, even though the burned-area maps derived from the two sensors exhibit a very high spatial correspondence, their spectral index

distributions differ substantially, as presented in Figs. 10 and 11. PS produces NDVI and dNDVI histograms that are systematically shifted toward higher values, a pattern evident both across the full scene (Fig. 10) and within the burned area (Fig. 11). These systematic differences reflect the influence of sensor-specific factors on vegetation index estimation and confirm that absolute NDVI or dNDVI values from the two sensors cannot be used interchangeably, as shown in Fig. 3, Fig. 5, and Fig. 10a.

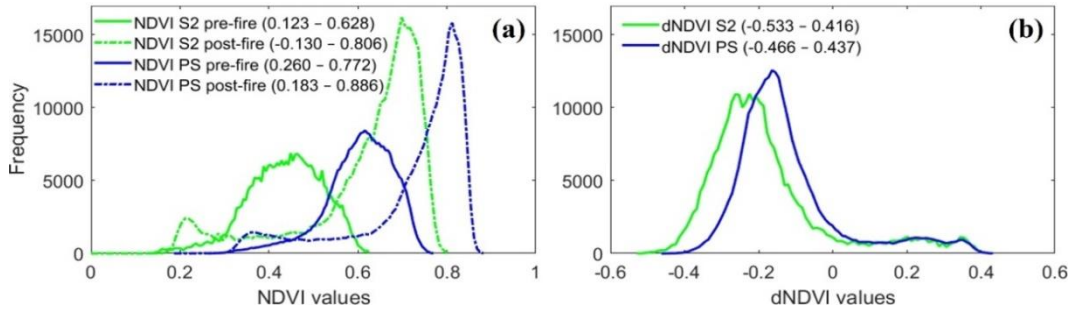

Figure 10. Histograms of NDVI (a) and dNDVI (b) before and after the fire event, derived from Sentinel-2 and PS imagery. Numbers in parentheses are NDVI and dNDVI ranges.

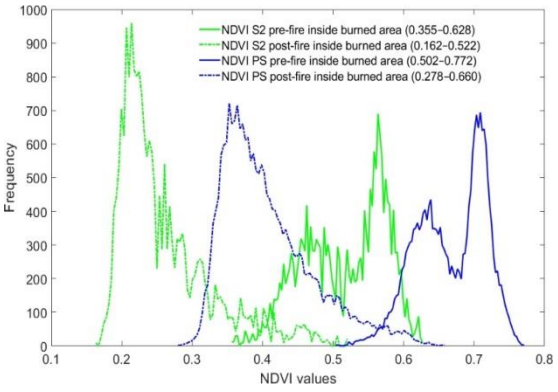

Figure 11. Histograms of NDVI within the burned area before and after the fire event, derived from Sentinel-2 and PS imagery. Numbers in parentheses are NDVI ranges.

Several factors can partly explain this difference, as already discussed in previous studies. First, differences in sensor design between Sentinel-2 and PS, including specific wavelength ranges, can lead to systematic differences in the Red and NIR bands, which directly affect the NDVI signal (Baldin & Casella, 2024a). Second, differences in spatial resolution play a critical role. With a higher spatial resolution of 3 m, PS sensors can capture purer vegetation signals and reduce mixed pixel effects. On the other hand, Sentinel-2 sensors with a 10 m spatial resolution tend to integrate reflectance from vegetation, soil, and ash into a single pixel, leading to a lower average NDVI distribution from Sentinel-2 compared to PS (do Amaral et al., 2023). Third, differences in atmospheric correction algorithms applied to the two datasets might further amplify their NDVI signals (Di Francesco et al., 2025). A potential solution to this problem is to apply histogram-matching techniques to harmonize the spectral reflectance between Sentinel-2 and PS imagery using radiometric intercalibration or linear regression (Baldin & Casella, 2024b, 2025). Histogram matching aligns the surface reflectance distribution of one dataset (e.g., PS) with that of a reference dataset (e.g., Sentinel-2), thereby reducing systematic differences in NDVI signals. In addition, data fusion of Sentinel-2 and PS imagery can improve the accuracy of burned-area mapping (Sadeh et al., 2021).

Despite the strong agreement in area estimates and fire-perimeter delineation, some limitations should be acknowledged. The reliance on cloud-free and temporally consistent images remains a critical requirement for optical approaches. In this

case study, the closest suitable pre- and post-fire scenes were acquired approximately two months before and after the fire event. Such a temporal separation introduces uncertainties into spectral change metrics and limits the operational applicability of the approach, particularly in cloud-prone environments (e.g., tropical and humid subtropical regions), where acquiring synchronous clear-sky imagery is inherently challenging. The absence of in situ reference data prevented quantitative validation of the classification results using standard accuracy metrics (e.g., confusion matrices, error budgets, or geolocation-based precision assessments).

Nevertheless, the high degree of agreement between the PS- and Sentinel-2-derived burned area estimates supports the internal consistency of the results. This is further corroborated by the fact that PS imagery is frequently employed as a high-resolution reference layer in fire-related remote sensing studies, owing to its 3-m pixel size and radiometric stability (Martins et al., 2022; Vetrita et al., 2025). Finally, it should be acknowledged that relying on a user-defined threshold may reduce the reproducibility of the proposed framework, particularly when applied to scenes characterized by varying radiometric and environmental conditions. A simple sensitivity test, performed by varying the threshold by ±0.05 around the reference value of 0.10, showed changes in the estimated burned area of up to 10%. The variability was slightly higher for PS data, as expected given its higher spatial resolution compared to Sentinel-2. Such fluctuations may affect overall detection accuracy and should therefore be carefully considered when assessing the method's broader applicability.

Future research should explore several directions. First, image fusion techniques should be investigated to combine the advantages of both sensors, namely, the high spatial and temporal resolution of PS and the spectral resolution of Sentinel-2, using methods presented in (Gašparović et al., 2018; Sadeh et al., 2021). Second, integrating unmanned aerial vehicle (UAV) imagery (Minh Khanh et al., 2024; Wicaksono et al., 2024) or very high-resolution satellite imagery (Ngo Van et al., 2025) could enhance validation efforts and support post-fire rehabilitation and conservation. Third, the potential of radar satellite data (e.g., Sentinel-1 imagery) for burned area mapping should be examined to reduce reliance on optical imagery and overcome limitations posed by cloud cover (Rokhmatuloh et al., 2022). Fourth, adopting a data-driven approach based on multitemporal satellite data analysis would enable the definition of automated, self-adaptive thresholds, thereby enhancing the reproducibility of burned-area segmentation across heterogeneous datasets (Satriano et al., 2023). Finally, extending the proposed approach to additional test sites characterized by diverse climatic conditions, land cover types, fire regimes, and integrating ground-based observations (e.g., field surveys or burn severity measurements), would allow a more robust evaluation of the method's generalizability and improve its applicability across different operational contexts.

6. Conclusions

This study compared the performance of multispectral optical sensors onboard PS and Sentinel-2 satellites in mapping burned areas associated with a small forest fire that occurred on 21 March, 2025, in Nghiem Mountain, northern Vietnam. Cloud-free pre- and post-fire images acquired by both satellites on the same dates (17 January and 12 May, 2025) were used to calculate the dNDVI from surface reflectance at the Red and NIR wavelengths. A user-defined threshold (T = 0.10), selected following a visual inspection of the dNDVI histograms, was applied to classify burned and unburned pixels. The results revealed a strong spatial correlation between the dNDVI maps derived

from PS and Sentinel-2 imagery (R = 0.97). Although Sentinel-2 sensors generally produced slightly higher dNDVI values than PS sensors, the burned-area estimates were remarkably similar: 20.622 ha for PS and 20.225 ha for Sentinel-2, corresponding to a difference of less than 2%. These values were also consistent with the ~20 ha of burned area as reported by local authorities. The high degree of spatial agreement between the two burned-area maps, particularly within the core of the affected region, highlights the reliability of both sensors for mapping small-scale fires, with discrepancies mostly restricted to transitional areas where mixed pixels introduce uncertainties. The findings confirm that medium- and high-resolution optical satellite imagery provides reliable and accurate burned-area estimates even for small-scale forest fires, offering essential support for effective forest management. Moreover, the approach adopted in this study demonstrates that such mapping can be achieved cost-effectively, making it particularly valuable for wildfire monitoring in rural or remote regions where on-site surveys are logistically challenging or resource-intensive. Looking ahead, integrating multi-sensor data fusion strategies, UAV-based validation, and radar observations could further enhance the robustness, temporal continuity, and operational applicability of burned-area mapping workflows, thereby strengthening future wildfire monitoring capabilities.

Acknowledgments

The authors gratefully acknowledge the European Space Agency and Planet's Education and Research Program for providing access to Sentinel-2 and PlanetScope satellites, respectively. The authors also thank Google for providing access to the Earth Engine cloud computing platform used for processing Sentinel-2 imagery. We thank the Editor and two anonymous reviewers for their valuable comments, which significantly improved the quality of the manuscript. This research was funded by the University of Science and Technology of Hanoi (USTH), grant number USTH.DSAE.01/26-27.

References

Amos C., Petropoulos G.P., Ferentinos K.P., 2019. Determining the use of Sentinel-2A MSI for wildfire burning & severity detection. International Journal of Remote Sensing, 40(3), 905–930. https://doi.org/10.1080/01431161.2018.1519284.

Balakavi S., Vadrevu V., Lasko K., 2025. Mapping burnt areas using very high-resolution imagery and deep learning algorithms - a case study in Bandipur, India. Plos One, 20(7), e0327125. https://doi.org/10.1371/journal.pone.0327125.

Baldin C.M., Casella V.M., 2024a. Comparison Between the Vegetation Indices Obtained from Sentinel-2 and Planet: A Case Study over a Rice Farm in Northern Italy. In: Borgogno Mondino, E., Zamperlin, P. (eds) Geomatics for Environmental Monitoring: From Data to Services. ASITA 2023. Communications in Computer and Information Science. Springer, Cham., 2088. https://doi.org/10.1007/978-3-031-59925-5_18.

Baldin C.M., Casella V.M., 2024b. Vegetative Index Intercalibration Between PlanetScope and Sentinel-2 Through a SkySat Classification in the Context of "Riserva San Massimo" Rice Farm in Northern Italy. Remote Sensing, 16(21), 3921. https://doi.org/10.3390/rs16213921.

Baldin C.M., Casella V.M., 2025. Comparison of PlanetScope and Sentinel-2 Spectral Channels and Their Alignment via Linear Regression for Enhanced Index Derivation. Geosciences, 15(5), 184. https://doi.org/10.3390/geosciences15050184.

Bar S., Parida B.R., Pandey A.C., 2020. Landsat-8 and Sentinel-2 based Forest fire burn area mapping using machine learning algorithms on GEE cloud platform over Uttarakhand, Western Himalaya. Remote Sensing Applications: Society and Environment, 18, 100324. https://doi.org/10.1016/j.rsase.2020.100324.

Bastarrika A., Rodriguez-Montellano A., Roteta E., Hantson S., Franquesa M., Torre L., Gonzalez-

Ibarzabal J., Artano K., Martinez-Blanco P., Mesanza A., Anaya J.A., Chuvieco E., 2024. An automatic procedure for mapping burned areas globally using Sentinel-2 and VIIRS/MODIS active fires in Google Earth Engine. ISPRS Journal of Photogrammetry and Remote Sensing, 218(Part A), 232–245. https://doi.org/10.1016/j.isprsjprs.2024.08.019.

Chen Y., Hall J., van Wees D., Andela N., Hantson S., Giglio L., van der Werf G.R., Morton D.C., Randerson J.T., 2023. Multi-decadal trends and variability in burned area from the fifth version of the Global Fire Emissions Database (GFED5). Earth System Science Data, 15(11), 5227–5259. https://doi.org/10.5194/essd-15-5227-2023.

Chuvieco E., Lizundia-Loiola J., Pettinari M.L., Ramo R., Padilla M., Tansey K., Mouillot F., Laurent P., Storm T., Heil A., Plummer S., 2018. Generation and analysis of a new global burned area product based on MODIS 250 m reflectance bands and thermal anomalies. Earth System Science Data, 10(4), 2015–2031. https://doi.org/10.5194/essd-10-2015-2018.

Chuvieco E., Mouillot F., van der Werf G.R., San Miguel J., Tanase M., Koutsias N., García M., Yebra M., Padilla M., Gitas I., Heil A., Hawbaker T.J., Giglio L., 2019. Historical background and current developments for mapping burned area from satellite Earth observation. Remote Sensing of Environment, 225, 45–64. https://doi.org/10.1016/j.rse.2019.02.013.

Di Francesco S., Biondi F., Casentini B., Fazi S., Amalfitano S., D'Eugenio M., Todisco F., Casadei S., Giannone F., 2025. Sentinel-2 and Planet-Scope as reliable tools for water quality monitoring of small reservoirs. The Egyptian Journal of Remote Sensing and Space Sciences, 28(4), 713–723. https://doi.org/10.1016/j.ejrs.2025.11.002.

do Amaral L.R., Oldoni H., Baptista G.M.M., Ferreira G.H.S., Freitas R.G., Stafford J.V., 2023. Vegetation indices from Sentinel-2 and PlanetScope imagery and their relationship with soybean yield. In Precision agriculture. Wageningen Academic, 23, 879–886. https://doi.org/10.3920/978-90-8686-947-3.

Dragozi E., Gitas I.Z., Stavrakoudis D.G., Minakou C., 2015. Burn severity estimation using GeoEye imagery, object-based image analysis (OBIA), and Composite Burn Index (CBI) measurements. In D. G. Hadjimitsis, K. Themistocleous, S. Michaelides, & G. Papadavid (Eds.), Third International Conference on Remote Sensing and Geoinformation of the Environment (RSCy2015). SPIE, 9535, 953515. https://doi.org/10.1117/12.2193149.

Frazier A.E., Hemingway B.L., 2021. A Technical Review of Planet Smallsat Data: Practical Considerations for Processing and Using PlanetScope Imagery. Remote Sensing, 13(19), 3930. https://doi.org/10.3390/rs13193930.

Gašparović M., Medak D., Pilaš I., Jurjević L., Balenović I., 2018. Fusion of Sentinel-2 and planetscope imagery for vegetation detection and monitoring. The International Archives of the Photogrammetry, Remote Sensing and Spatial Information Sciences, XLII–1, 155–160. https://doi.org/10.5194/isprs-archives-XLII-1-155-2018.

Gibson R., Danaher T., Hehir W., Collins L., 2020. A remote sensing approach to mapping fire severity in south-eastern Australia using sentinel 2 and random forest. Remote Sensing of Environment, 240, 111702. https://doi.org/10.1016/j.rse.2020.111702.

Giglio L., Boschetti L., Roy D.P., Humber M.L., Justice C.O., 2018. The Collection 6 MODIS burned area mapping algorithm and product. Remote Sensing of Environment, 217, 72–85. https://doi.org/10.1016/j.rse.2018.08.005.

Gorelick N., Hancher M., Dixon M., Ilyushchenko S., Thau D., Moore R., 2017. Google Earth Engine: Planetary-scale geospatial analysis for everyone. Remote Sensing of Environment, 202, 18–27. https://doi.org/10.1016/j.rse.2017.06.031.

Hawbaker T.J., Vanderhoof M.K., Schmidt G.L., Beal Y.-J., Picotte J.J., Takacs J.D., Falgout J.T., Dwyer J.L., 2020. The Landsat Burned Area algorithm and products for the conterminous United States. Remote Sensing of Environment, 244, 111801. https://doi.org/10.1016/j.rse.2020.111801.

Hitchcock H.C., Hoffer R.M., 1974. Mapping a recent forest fire with ERTS-1 MSS data. Remote sensing of earth resources. Volume 3-Third Conference on Earth Resources Observation and Information Analysis System.

Howe A.A., Parks S.A., Harvey B.J., Saberi S.J., Lutz J.A., Yocom L.L., 2022. Comparing Sentinel-2 and Landsat 8 for Burn Severity Mapping in Western North America. Remote Sensing, 14(20), 5249. https://doi.org/10.3390/rs14205249.

Jones M.W., Abatzoglou J.T., Veraverbeke S., Andela N., Lasslop G., Forkel M., Smith A.J.P., Burton C., Betts R.A., van der Werf G.R., Sitch S., Canadell J.G., Santín C., Kolden C., Doerr S.H., Le Quéré C., 2022. Global and Regional Trends and Drivers of Fire Under Climate Change. Reviews of Geophysics, 60(3), e2020RG000726. https://doi.org/10.1029/2020RG000726.

Key C.H., Benson N.C., 2003. The Normalized Burn Ratio (NBR): A Landsat TM radiometric measure of burn severity, US Department of the Interior. US Geological Survey, Northern Rocky Mountain Science Center.

Kim M., Jung M., Kim Y., 2019. Histogram Matching of Sentinel-2 Spectral Information to Enhance Planetscope Imagery for Effective Wildfire Damage Assessment. Korean Journal of Remote Sensing, 35(4), 517–534. https://doi.org/10.7780/kjrs.2019.35.4.3.

Konkathi P., Shetty A., 2021. Inter comparison of post-fire burn severity indices of Landsat-8 and Sentinel-2 imagery using Google Earth Engine. Earth Science Informatics, 14(2), 645–653. https://doi.org/10.1007/s12145-020-00566-2.

Lao-Dong, 2025. Tuyen Quang issues directive document after catastrophic forest fire. https://news.laodong.vn/thoi-su/tuyen-quang-ra-van-ban-chi-dao-sau-vu-chay-rung-tham-khoc-1481041.ldo.

Lasko K., 2021. Incorporating Sentinel-1 SAR imagery with the MODIS MCD64A1 burned area product to improve burn date estimates and reduce burn date uncertainty in wildland fire mapping. Geocarto International, 36(3), 340–360. https://doi.org/10.1080/10106049.2019.1608592.

Liu P., Liu Y., Guo X., Zhao W., Wu H., Xu W., 2023. Burned area detection and mapping using time series Sentinel-2 multispectral images. Remote Sensing of Environment, 296, 113753. https://doi.org/10.1016/j.rse.2023.113753.

Marín P.-G., Julio C.J., Dante Arturo R.-T., Daniel Jose V.-N., 2018. Drought and Spatiotemporal Variability of Forest Fires Across Mexico. Chinese Geographical Science, 28(1), 25–37. https://doi.org/10.1007/s11769-017-0928-0.

Martins V.S., Roy D.P., Huang H., Boschetti L., Zhang H.K., Yan L., 2022. Deep learning high resolution burned area mapping by transfer l earning from Landsat-8 to PlanetScope. Remote Sensing of Environment, 280, 113203. https://doi.org/10.1016/j.rse.2022.113203.

Minh Khanh L., Tong Si S., Mai H., To Thi Mai H., Tran Son G., Pham-Duc B., Phan H., Le Van C., Pham Thi L., Tong Thi Huyen A., 2024. UAV hyperspectral image acquisition and processing, an application for nutrient estimation of rice in Vietnam. Vietnam Journal of Earth Sciences, 46(4), 533–552. https://doi.org/10.15625/2615-9783/21306.

Moreira F., Ascoli D., Safford H., Adams M.A., Moreno J.M., Pereira J.M.C., Catry F.X., Armesto J., Bond W., González M.E., Curt T., Koutsias N., McCaw L., Price O., Pausas J.G., Rigolot E., Stephens S., Tavsanoglu C., Vallejo V.R., Fernandes P.M., 2020. Wildfire management in Mediterranean-type regions: paradigm change needed. Environmental Research Letters, 15(1), 11001. https://doi.org/10.1088/1748-9326/ab541e.

Mouillot F., Field C.B., 2005. Fire history and the global carbon budget: a 1°× 1° fire history reconstruction for the 20th century. Global Change Biology, 11(3), 398–420. https://doi.org/10.1111/j.1365-2486.2005.00920.x.

Ngo Van L., Nguyen H., Dang Kinh B., Giang Tuan L., Dang Van B., Do Trung H., Nguyen Minh H., Dang Nguyen V., Dao Minh D., 2025. Advancing debris flow detection based on deep learning model and high-resolution images. Vietnam Journal of Earth Sciences, 47(2), 290–314. https://doi.org/10.15625/2615-9783/23027.

Nguyen Cong G., Nguyen Quyet C., Dang Vu K., 2024. Estimation of greenhouse gas emission due to open burning of rice straw using Sentinel data. Vietnam Journal of Earth Sciences, 46(3), 381–398. https://doi.org/10.15625/2615-9783/20716.

Nguyen Thanh H., Ho Le T., Nguyen Van D., Hoa Thuy Q., Nguyen Kim A., Le Duc H., Pham Van D., Phan Trong T., Tran Van P., 2025. Forest cover change mapping based on Deep Neuron Network, GIS, and High-resolution Imagery. Vietnam Journal of Earth Sciences, 47(2), 157–181. https://doi.org/10.15625/2615-9783/22192.

Or D., Furtak-Cole E., Berli M., Shillito R., Ebrahimian H., Vahdat-Aboueshagh H., McKenna S.A., 2023. Review of wildfire modeling considering effects on land surfaces. Earth-Science Reviews, 245, 104569. https://doi.org/10.1016/j.earscirev.2023.104569.

Ouattara B., Thiel M., Sponholz B., Paeth H., Yebra M., Mouillot F., Kacic P., Hackman K., 2024. Enhancing burned area monitoring with VIIRS dataset: A case study in Sub-Saharan Africa. Science of Remote Sensing, 10, 100165. https://doi.org/10.1016/j.srs.2024.100165.

Palandjian D., Gitas I.Z., Wright R., 2009. Burned area mapping and post-fire impact assessment in the Kassandra peninsula (Greece) using Landsat TM and Quickbird data. Geocarto International, 24(3), 193–205. https://doi.org/10.1080/10106040802488542.

Paquette A., Vayreda J., Coll L., Messier C., Retana J., 2018. Climate Change Could Negate Positive Tree Diversity Effects on Forest Productivity. Ecosystems, 21(5), 960–970. https://www.jstor.org/stable/48719583.

Pereira A.A., Pereira J.M.C., Libonati R., Oom D., Setzer A.W., Morelli F., Machado-Silva F., De Carvalho L.M.T., 2017. Burned Area Mapping in the Brazilian Savanna Using a One-Class Support Vector Machine Trained by Active Fires. Remote Sensing, 9(11), 1161. https://doi.org/10.3390/rs9111161.

Pereira P., Bogunovic I., Zhao W., Barcelo D., 2021. Short-term effect of wildfires and prescribed fires on ecosystem services. Current Opinion in Environmental Science & Health, 22, 100266. https://doi.org/10.1016/j.coesh.2021.100266.

Pham Thanh T., Chu T., Tran Quang B., 2024. Modelling spatial patterns of forest fire occurrence in the Northwestern region of Vietnam. Vietnam Journal of Earth Sciences, 46(2), 282–302. https://doi.org/10.15625/2615-9783/20366.

Pham-Duc B., 2023. Mapping small burned areas using high spatial resolution planetscope imagery: a case study of the wildfire in Da Lat city. Journal of Forestry Science and Technology, 8(2), 97–106. https://doi.org/10.55250/jo.vnuf.8.2.2023.097-106.

Pham-Duc B., Nguyen H., 2024. Remote sensing assessment of wildfire using high-resolution PlanetScope satellite observations: A case study on Co Tien Mountain, Nha Trang City, Vietnam. Journal of Degraded and Mining Lands Management, 12(1), 6491–6499. https://doi.org/10.15243/jdmlm.2024.121.6491.

Pham-Duc B., Nguyen H., Nguyen-Quoc H., 2024. Unveiling the research landscape of planetscope data in addressing earth-environmental issues: a bibliometric analysis. Earth Science Informatics, 18(1), 52. https://doi.org/10.1007/s12145-024-01497-y.

Pham-Duc B., Nguyen H., Phan H., Tran-Anh Q., 2023. Trends and applications of google earth engine in remote sensing and earth science research: a bibliometric analysis using scopus database. Earth Science Informatics, 16(3), 2355–2371. https://doi.org/10.1007/s12145-023-01035-2.

Radeloff V.C., Helmers D.P., Kramer H.A., Mockrin M.H., Alexandre P.M., Bar-Massada A., Butsic V., Hawbaker T.J., Martinuzzi S., Syphard A.D., Stewart S.I., 2018. Rapid growth of the US wildland-urban interface raises wildfire risk. Proceedings of the National Academy of Sciences, 115(13), 3314–3319. https://doi.org/10.1073/pnas.1718850115.

Rokhmatuloh, Ardiansyah, Indratmoko S., Riyanto I., Margatama L., Arief R., 2022. Burnt-Area Quick Mapping Method with Synthetic Aperture Radar Data. Applied Sciences, 12(23), 11922. https://doi.org/10.3390/app122311922.

Sadeh Y., Zhu X., Dunkerley D., Walker J.P., Zhang Y., Rozenstein O., Manivasagam V.S., Chenu K., 2021. Fusion of Sentinel-2 and PlanetScope time-series data into daily 3 m surface reflectance and wheat LAI monitoring. International Journal of Applied Earth Observation and Geoinformation, 96, 102260. https://doi.org/10.1016/j.jag.2020.102260.

Satriano V., Ciancia E., Filizzola C., Genzano N., Lacava T., Tramutoli V., 2023. Landslides Detection

and Mapping with an Advanced Multi-Temporal Satellite Optical Technique. Remote Sensing, 15(3), 683. https://doi.org/10.3390/rs15030683.

Seydi S.T., Akhoondzadeh M., Amani M., Mahdavi S., 2021. Wildfire Damage Assessment over Australia Using Sentinel-2 Imagery and MODIS Land Cover Product within the Google Earth Engine Cloud Platform. Remote Sensing, 13(2), 220. https://doi.org/10.3390/rs13020220.

Spoto F., Sy O., Laberinti P., Martimort P., Fernandez V., Colin O., Hoersch B., Meygret A., 2012. Overview Of Sentinel-2. 2012 IEEE International Geoscience and Remote Sensing Symposium, 1707–1710. https://doi.org/10.1109/IGARSS.2012.6351195.

Suárez-Fernández G.E., Martínez-Sánchez J., Arias P., 2025. Assessment of vegetation indices for mapping burned areas using a deep learning method and a comprehensive forest fire dataset from Landsat collection. Advances in Space Research, 75(2), 1665–1685. https://doi.org/10.1016/j.asr.2024.12.001.

Suwanprasit C., Shahnawaz., 2024. Mapping burned areas in Thailand using Sentinel-2 imagery and OBIA techniques. Scientific Reports, 14(1), 9609. https://doi.org/10.1038/s41598-024-60512-w.

Szpakowski D.M., Jensen J.L.R., 2019. A Review of the Applications of Remote Sensing in Fire Ecology. Remote Sensing, 11(22). https://doi.org/10.3390/rs11222638.

UN-SPIDER, 2023. Normalized Burn Ratio (NBR). https://www.un-spider.org/advisory-support/recommended-practices/recommended-practice-burn-severity/in-detail/normalized-burn-ratio.

Vanderhoof M.K., Burt C., Hawbaker T.J., 2018. Time series of high-resolution images enhances efforts to monitor post-fire condition and recovery, Waldo Canyon fire, Colorado, USA. International Journal of Wildland Fire, 27(10), 699–713. doi.org/10.1071/WF17177.

Vetrita Y., Diwyacitta K., Sukarno K. M., Albar I., Usman A.B., Ritonga R.P., Santoso I., Lestari A.I., Kartika T., Novresiandi D.A., Prasasti I., Ulfa K., Novita N., Siwi S.E., Augusto S., Prakoso E.T., Rahmi K.I.N., Nugroho U.C., Widodo J., Cochrane M.A., 2025. Evaluating the capabilities of high-resolution PlanetScope and Sentinel-2 images for mapping burned area and vegetation regrowth in Indonesia's savannas. International Journal of Remote Sensing, 46(18), 6803–6825. https://doi.org/10.1080/01431161.2025.2546154.

Wicaksono P., Hafizt M., Harahap S.D., Nandika M.R., 2024. Integrating Sentinel-2 and PlanetScope Image with Drone-based Seagrass Data for Seagrass Percent Cover Mapping. IOP Conference Series: Earth and Environmental Science, 1291(1), 12012. https://doi.org/10.1088/1755-1315/1291/1/012012.

Zhang P., Ban Y., Nascetti A., 2021. Learning U-Net without forgetting for near real-time wildfire monitoring by the fusion of SAR and optical time series. Remote Sensing of Environment, 261, 112467. https://doi.org/10.1016/j.rse.2021.112467.

Zhang P., Hu X., Ban Y., Nascetti A., Gong M., 2024. Assessing Sentinel-2, Sentinel-1, and ALOS-2 PALSAR-2 Data for Large-Scale Wildfire-Burned Area Mapping: Insights from the 2017–2019 Canada Wildfires. Remote Sensing, 16(3), 556. https://doi.org/10.3390/rs16030556.